Available online at www.sciencedirect.com

SciVerse ScienceDirect

Solar Energy 89 (2013) 42–53

SOLAR ENERGY

www.elsevier.com/locate/solener

Neural-network-based maximum power point tracking methods for photovoltaic systems operating under fast changing environments

Yi-Hua Liu [a,*], Chun-Liang Liu [a], Jia-Wei Huang [b], Jing-Hsiau Chen [a]

[a] Department of Electrical Engineering, National Taiwan University of Science and Technology, Taiwan
[b] System Application Department, Photovoltaic Technology Division, Green Energy and Environment Research Laboratories, Industrial Technology Research Institute, Taiwan

Received 23 August 2012; received in revised form 25 November 2012; accepted 26 November 2012
Available online 19 January 2013

Communicated by: Associate Editor Nicola Romeo

Abstract

Photovoltaic (PV) generation systems (PGSs) have become an attractive option among renewable energy sources because they are clean, maintenance-free and environmental friendly. For PGSs, a simple and fast maximum power point tracking (MPPT) algorithm is essential. Although the static tracking efficiency of conventional MPPT method is usually high, it drops noticeably in case of rapidly changing irradiance conditions. In this paper, two fast and accurate digital MPPT methods for fast changing environments are proposed. By using piecewise line segments or cubic equation to approximate the maximum power point (MPP) locus, two high-speed, low-complexity MPPT techniques can be developed. To make the developed system more convenient for common PGS users, neural network (NN)-based program which can be used to calculate the parameters of the emulated MPP locus is also developed and embedded into the proposed digital MPPT system. Theoretical derivation and detailed design procedure will be provided in this paper. The advantages of the proposed system include low computation requirement, fast tracking speed and high static/dynamic tracking efficiencies. To validate the effectiveness and correctness of the proposed methods, simulation and experimental results of a 230 W PV system will also be provided.

Keywords: Photovoltaic (PV); Maximum power point tracking (MPPT); Neural network

1. Introduction

Due to continuous growth of global energy demand and increasing concern about environmental issues, interests on using and developing renewable energy sources are growing. Among those energy sources, the photovoltaic (PV) technology is an attractive option because it features several advantages such as absence of fuel cost, low maintenance requirement and environmental friendliness. The energy conversion efficiency of a PV generation system (PGS) is low because the solar cell exhibits nonlinear current versus voltage (I–V) and power versus voltage (P–V) characteristics. These nonlinear characteristics are functions of weather conditions such as solar insolation and panel temperature. In order to maintain efficient operation, a maximum power point tracking (MPPT) algorithm which has quick response and can extract maximum power from the PV arrays in real time becomes essential in PGSs (Chekired et al., 2011; Du and Lu, 2011; Kakosimos and Kladas, 2011; Lalili et al., 2011; Ko and Chao, 2012). Many MPPT techniques have been proposed and implemented. These

* Corresponding author. Address: Department of Electrical Engineering, National Taiwan University of Science and Technology, No. 43, Sec. 4, Keelung Road, Taipei 106, Taiwan, R.O.C. Tel.: +886 27301252; fax: +886 27376699.
E-mail addresses: yhliu@mail.ntust.edu.tw (Y.-H. Liu), D10007201@mail.ntust.edu.tw (C.-L. Liu), J.W.Huang@itri.org.tw (J.-W. Huang), D10107201@mail.ntust.edu.tw (J.-H. Chen).

0038-092X/$ - see front matter © 2012 Elsevier Ltd. All rights reserved.
http://dx.doi.org/10.1016/j.solener.2012.11.017

methods include perturb and observe (P&O), incremental conductance (IncCon), fractional open-circuit voltage, fractional short-circuit current, fuzzy logic control (FLC) and ripple correlation control (RCC) approaches. Some modified techniques which aim to minimize the hardware requirement or to improve the performance have also been proposed (Hohm and Ropp, 2003; Salas et al., 2006; Esram and Chapman, 2007). When the operating conditions of the PV array are smooth and stable, these conventional MPPT methods can provide high performance tracking. However, on places where the irradiation changes rapidly due to changing atmospheric conditions such as clouds, the overall tracking efficiency of the conventional techniques may drop noticeably. For example, P&O method has been shown to track in the wrong direction under sudden increase/decrease of irradiance if the effect of irradiance change is greater than that of the perturbation step applied. Moreover, if the dynamic of the utilized MPPT algorithm is slower than the speed of irradiation changes, the overall maximum power point (MPP) tracking efficiency will become lower since the MPP cannot be tracked accurately at every moment. Therefore, a fast and accurate MPPT method is required (Pandey et al., 2008; Sera et al., 2008; Andrejašič et al., 2011).

Many MPPT techniques suitable for fast changing environments have been proposed in both analog and digital forms. Detailed discussion about the advantages and disadvantages of analog MPPT methods is presented in Liu and Huang (2011). From Liu and Huang (2011), analog MPPT methods provide faster response than digital ones because the bandwidth of the analog loop is higher. However, most analog MPPT methods require analog multipliers which are expensive and power-hungry. On the other hand, many low-cost, low-power microcontrollers (μC) with built-in hardware digital multipliers are available from IC vendors such as Texas Instruments and Microchip. Therefore, digital implementation of MPPT is preferable in medium and high power PV systems where digital controllers are commonly utilized. In addition, digital implementation enables features such as protection modes and user interfaces. Some researchers have worked on digital MPPT schemes suitable for fast changing environments. In Masoum et al. (2002), a voltage-based MPPT and a current-based MPPT approaches are presented. Both methods are simple and fast. However, these methods present poor tracking efficiencies for low irradiation levels. In Jain and Agarwal (2004), a new method is proposed based on the analysis and derivation of the I–V characteristics of a PV panel by defining a natural logarithmic index. This method can provide faster tracking speed than the conventional hill-climbing method, but the utilized index is too complicate for real-time calculation using an inexpensive 8- or 16-bit μC. In Mutoh et al. (2006), MPPT control rules are created based on a prediction line that associates the MPP and the optimum current. One of its parameter (voltage coefficient) should be acquired through the hill-climbing method, which makes it commercially impractical. Kimball and Krein (2008) extend the previous analog RCC technique to the digital domain for MPP tracking. The proposed digital implementation is less expensive, more flexible, and more robust. Similar to analog RCC method, the inductive and capacitive parasitic components may have a significant impact on the ability of RCC to drive the system toward the true MPP. To deal with the tradeoff between the steady-state performance and the speed of the tracking, steepest descent method, variable step-size methods, parabolic prediction technique and FLC-based approach are also proposed for MPP tracking (Xiao et al., 2007; Liu et al., 2008; Pandey et al., 2008; Abdelsalam et al., 2011; Alajmi et al., 2011; Mei et al., 2011; Pai et al., 2011; Elgendy et al., 2012). These methods show faster dynamic response and smoother steady state than conventional MPPT algorithms. However, these methods all utilize two output power samples corresponding to two steady-state operating points to determine the incremental value of the control variable. Therefore, when the operating point is adjusted, the system must wait for all transients to settle before recording information. Thus, the tracking speed of these methods is limited by the dynamics of the system. Extreme seeking (ES) controller is proposed in Brunton et al. (2010), which offers fast convergence and good steady-state performance with guaranteed stability for a range of parameters. Similar to RCC method, ES controller requires voltage and current ripple information, which are only a few percent of the average voltage and current. Therefore, high resolution analog to digital converter (ADC) is required, which increase the cost of the system. A less complicate way of tracking the MPP is through an estimation technique, based on an offline module characterization. In Sokolov and Shmilovitz (2008), the relationship between the values of panel voltage and current at the MPP (one virtual load line) is used to accelerate the speed of the MPPT algorithm. Since the actual MPP loci are not on a straight line, P&O method is additionally utilized to obtain the real MPP.

In this paper, two simple and fast MPPT methods suitable for fast changing environments are proposed. The concept presented in Liu and Huang (2011) is extended to digital domain. The presented techniques model the nonlinear I–V characteristics of the solar panel using numerical approximations. To improve the tracking efficiency, polynomial interpolation technique is employed to emulate the MPP locus. Two emulation results – piecewise line segments (PLSs) and cubic equation (CE) – are utilized to accurately model the MPP locus. The proposed approach is simple because the calculation of the voltage command only requires a few multiplications and additions. After the voltage command is obtained, a separate high-speed voltage loop can then be applied to regulate the PV panel output voltage to follow the emulated MPP locus (EML). The voltage loop provides a fast response to sudden changes of irradiance levels and hence helps to improve the dynamic MPP tracking efficiency.

The basic design principle of the proposed method is to operate the MPP of the PV panel along the EML. To obtain the EML, the PV panel parameters are required. However, some of the parameters required for numerical simulation are not usually available in the manufacturer's datasheets. Moreover, many PGS users don't possess the knowledge and the skills to modify the firmware of the PGS. Therefore, to assist the PGS users, a neural network (NN)-based program which can be used to automatically calculate the parameters of the EML is also developed. The NN method has been successfully employed to solve different engineering modeling problems (Chen et al., 2011; Lee et al., 2011; Kassem, 2012; Leconte et al., 2012; Syafaruddin et al., 2012). According to these investigations, NNs have the ability to model linear and non-linear systems without the need to make assumptions implicitly as in most traditional statistical approaches. The developed NN will be embedded into the proposed digital controller. Using this scheme, PGS users can input the solar panel parameters using a graphical user interface (GUI), and the proposed digital MPPT system will automatically calculate the EML parameters and perform the MPP tracking accordingly. Detailed description of the developed NN model will be presented in Section 4. Finally, simulation and experimental results will be provided to validate the feasibility and effectiveness of the proposed method. From the simulation and experimental results, the proposed method is fast, accurate and flexible.

2. Solar cell characteristics and MPPT testing techniques

2.1. Solar cell characteristics

Fig. 1 shows the equivalent circuit of the PV cell. The basic equation that mathematically describes the $I-V$ characteristic of the PV cell is

$$I_{pv} = I_g - I_S\left(\exp\left(\frac{q(V_{pv}+I_{pv}\cdot R_S)}{nkT}\right)-1\right) \quad (1)$$

where n is the ideality factor, k is the Boltzmann's constant, q is the electron charge, T is the temperature in Kelvin, R_S is the equivalent series resistance and I_g, I_{pv} and I_s are the photogenerated current, panel current and saturation currents, respectively.

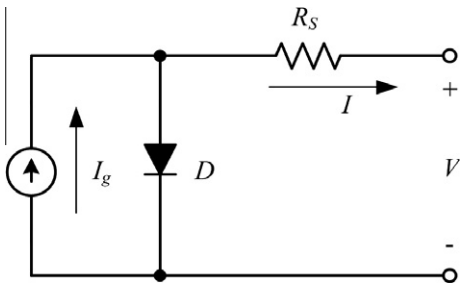

Fig. 1. Equivalent circuit of the PV cell.

2.2. MPPT testing for fast changing environments

The performance of the MPPT algorithm can be measured both in static and dynamic ways; the static MPP tracking efficiency depicts the ability of the MPPT algorithm to find and hold the MPP under constant environmental conditions (i.e., solar irradiance and panel temperature) whereas the dynamic MPP tracking efficiency describes the ability in tracking the MPP under variable environmental conditions. The static MPP tracking efficiency η_{STATIC} is defined as

$$\eta_{STATIC} = \frac{P_O}{P_{MAX}} \times 100\% \quad (2)$$

where P_O is the averaged output power obtained under steady state and P_{MAX} is the maximum available power of the PV panel under certain environmental conditions.

At locations where the irradiation changes rapidly due to changing atmospheric conditions, both the static and the dynamic MPP tracking efficiency have to be considered. PGSs with a fast MPP tracker will have higher energy yield under fast changing environments than the ones with slow MPP tracking scheme. Therefore, The MPPT testing has to include not only its performance at two or more different irradiance levels, but also how it tracks the MPP during the transients. Measuring the dynamic MPP tracking efficiency has not been standardized until the European Standard EN50530:2010 was published (EN 50530, 2010). In EN50530:2010, the dynamic MPP tracking efficiency is determined by two test sequences of different irradiance level. Fig. 2 depicts the general test pattern for the dynamic MPPT tests. In Fig. 2, t_1 is the rise time, t_2 is the dwell time on high irradiation level, t_3 is the fall time, t_4 is the dwell time on low irradiation level, n is the repetition number, G is the irradiation level under test, and G_{STC} is the irradiation level for standard test conditions ($G_{STC} = 1000$ W/m^2) (EN 50530, 2010). From Fig. 2, the test sequence starts with an initial setup time that is followed by repeating patterns with a trapezoidal shape. This shape varies during the test. The dynamic MPP tracking efficiency $\eta_{DYNAMIC}$ can be defined as

$$\eta_{DYNAMIC} = \frac{\int_0^T v_{PV}(t)\cdot i_{PV}(t)dt}{\int_0^T P_{MAX}(t)dt} \times 100\% \quad (3)$$

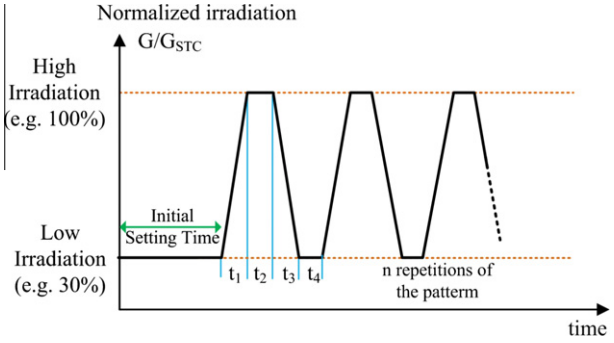

Fig. 2. General test pattern for the dynamic MPPT tests.

where $v_{PV}(t)$ and $i_{PV}(t)$ represent the measured instantaneous voltage and current at the output of the PV panel. The $P_{MAX}(t)$ represents the available maximum power of the PV panel. T represents the time duration of the whole test sequence.

3. Derivation of the proposed method

In this section, the derivation of the proposed method will be provided. To simplify the design procedure, numerical method instead of analytical technique is employed to obtain the EML in this paper. For PV panels, the MPP locus can be defined as the point (V_{MP}, I_{MP}), which expresses a function of panel irradiation at a given operating temperature. Fig. 3 shows the I–V curves of the utilized NU-U230F3 (from SHARP Corp.) solar panel under different irradiation levels, which are obtained using MATLAB simulation. In this paper, Eq. (1) is utilized to model the solar cell. The circular markers in the graphs represent the calculated MPP points (V_{MP}, I_{MP}). From Fig. 3a, the MPP locus can be modeled as two line segments. Using this concept, the EML can be written as

$$\begin{cases} V_{PV} = k_{HIGH} I_{PV} + V_{OFFSET,H}, & V_{PV} \geqslant V_{TP} \\ V_{PV} = k_{LOW} I_{PV} + V_{OFFSET,L}, & V_{PV} < V_{TP} \end{cases} \tag{4}$$

In Eq. (4), the slope k and the offset point V_{OFFSET} are different for high and low irradiation conditions, and V_{TP} is the turning point voltage which determines whether the irradiation level is high or low. In summary, if the I–V characteristics for any PV panel can be obtained, the parameter set (k_{HIGH}, k_{LOW}, $V_{OEESET,H}$, $V_{OFFSET,L}$) of the EML can be calculated using the polynomial curve fitting function *polyfit* from MATLAB by setting the degree of polynomial as 2.

Observing Fig. 3b, the EML can also be modeled as a cubic equation as shown in Eq. (5). In Eq. (5), the parameter set (a, b, c, V_{OFFSET}) determines the shape of the cubic equation. Similarly, the parameter sets (a, b, c, V_{OFFSET}) of the EML can be obtained using the *polyfit* function by setting the degree of polynomial as 4.

$$V_{PV} = aI_{PV}^3 + bI_{PV}^2 + cI_{PV} + V_{OFFSET} \tag{5}$$

Fig. 4 depicts the block diagram of the proposed system. From Fig. 4, the reference voltage command $V_M^* P$ is calculated using Eq. (4) or Eq. (5), and is then fed into a high-speed voltage regulating loop (typically $\geqslant$ 50 kHz). As in other MPPT methods, in order to acquire correct samples, the time interval between successive samples has to be greater than the system's settling time. Therefore, the perturbation frequency should be low enough so that the system can reach a steady state before the next perturbation (Elgendy et al., 2012). Typically, the value of perturbation frequency (f_{MPPT}) lies between 1 Hz and 1 kHz. When the PGS is subjected to a step change in irradiation level, conventional P&O methods require a few perturbation steps to reach the MPPT value. On the other hand, the operation along the EML is carried out by the fast voltage regulating loop. Thus, the tracking time of the proposed method can be greatly reduced. In addition, this voltage regulating loop is commonly utilized in switching power converters and can simply be implemented using a commercially available pulse-width modulated (PWM) IC in analog form. For

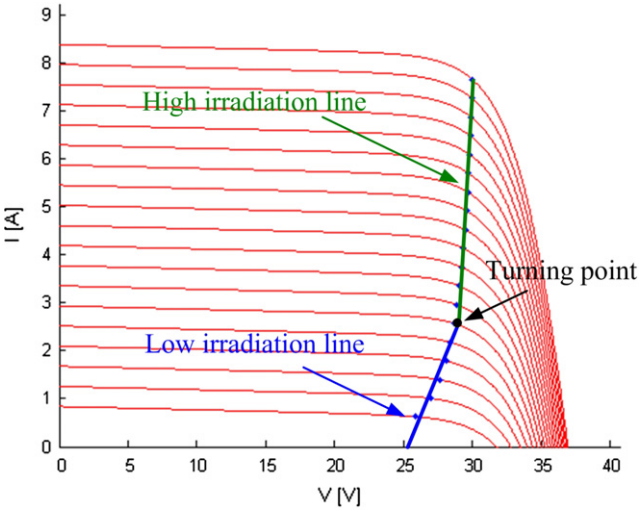

(a) Piecewise line segment approximation.

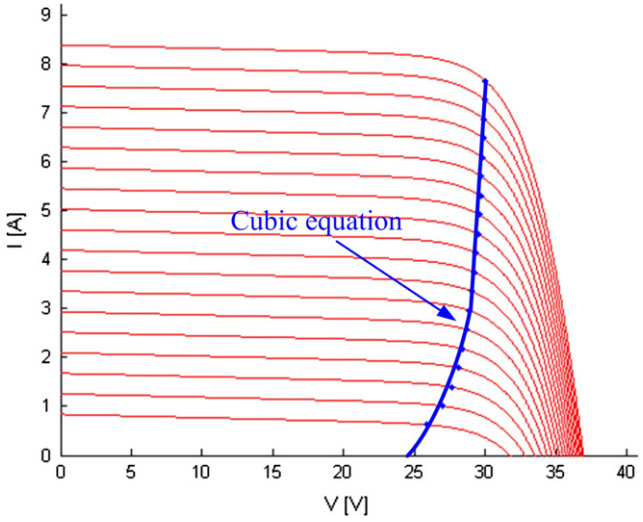

(b) Cubic equation approximation.

Fig. 3. I–V curves of the utilized solar panel under different irradiation levels.

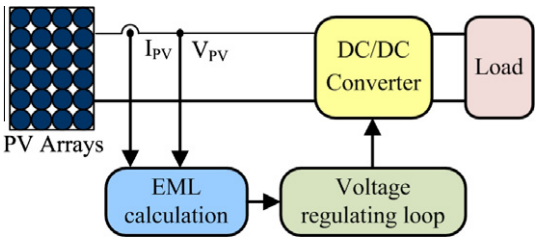

Fig. 4. The block diagram of the proposed system.

digital implementation, this voltage regulation loop can also easily be integrated into the digital controller. Moreover, once the equilibrium point is reached, a further increase/decrease of the current will be prevented by the voltage regulating loop. As a result, phenomena like oscillations around the MPP or control losses due to sudden irradiation variations will not occur. Therefore, higher tracking efficiency can be achieved.

4. Development of a NN-based method for obtaining the parameters of EML

From Section 3, the parameter sets emulating the MPP locus can be obtained using the *I–V* characteristic curves of the solar cell. However, some of the parameters required for numerical simulation are not usually available in the manufacturer's datasheets. For example, the series resistances R_s, the diode ideality constant n and the diode reverse saturation current I_s in Eq. (1) are typically not provided by the PV panel manufacturer. Basically, the only information one can get from datasheets of PV panels are: the nominal open-circuit voltage ($V_{OC,STC}$), the nominal short-circuit current ($I_{SC,STC}$), the voltage at the MPP (V_{MP}), the current at the MPP (I_{MP}) and the number of series cells (N_s). Therefore, an effective method which can be used to obtain the parameters of the *I–V* equation from practical data available in datasheets is required. In this paper, the technique proposed in Villalva et al. (2009) is utilized. To assist the system designer, a MATLAB-based program which can be used to automatically calculate the parameters of the EML is also developed. The developed program can be found at https://sites.google.com/site/d9707203/code.

Using the presented MATLAB program, PGS design engineers can input the specification data from the datasheet to obtain the parameters of EML, and then modify the MPPT program accordingly. However, for common PGS users who are not acquainted with MATLAB and μC programming, this becomes a troublesome task. Therefore, to make the proposed MPPT system more convenient, a NN-based program which can be used to automatically calculate the parameters of the EML is also developed. Using the developed NN model, the PGS user can apply the developed MPPT controller to any PV panel without the need to modify the firmware of the PGS. In this study, to map the relationship between the EML parameter sets and the data available from the datasheet, a three layer feedforward NN as shown in Fig. 5 is utilized. The input layer in this study consists of a five dimensional vector ($V_{OC,STC}$, $I_{SC,STC}$, V_{MP}, I_{MP}, N_s) and the output vector is a four dimensional vector comprising EML parameters ((k_{HIGH}, k_{LOW}, $V_{OEESET,H}$, $V_{OFFSET,L}$) or (a, b, c, V_{OFFSET})). The number of hidden layer nodes is determined empirically. The 10 hidden nodes give the most accurate estimation; therefore, only the results of this case are given in the paper. To sum up, the input layer has 5 nodes, the hidden layer has 10 nodes and the output layer has 4 nodes (see Fig. 5). From Fig. 5, the relationships between the inputs and outputs are given as follows:

Neurons in input layer only act as buffers for distributing the input signals. The net input of the j-th hidden unit is

$$n_j^1 = \sum_{i=1}^{5} w_{ji} u_i + b_j^1, \quad j = 1\text{–}10 \tag{6}$$

where w_{ji} is the weighting on the connection from the i th input unit, b_j^1 represent the bias for the hidden layer neurons. The output of the neurons in the hidden layer is

$$v_j = f_1(n_j^1), \quad f_1(x) = purelin(x) = x \tag{7}$$

and the net input to the neurons in the output layer can be written as

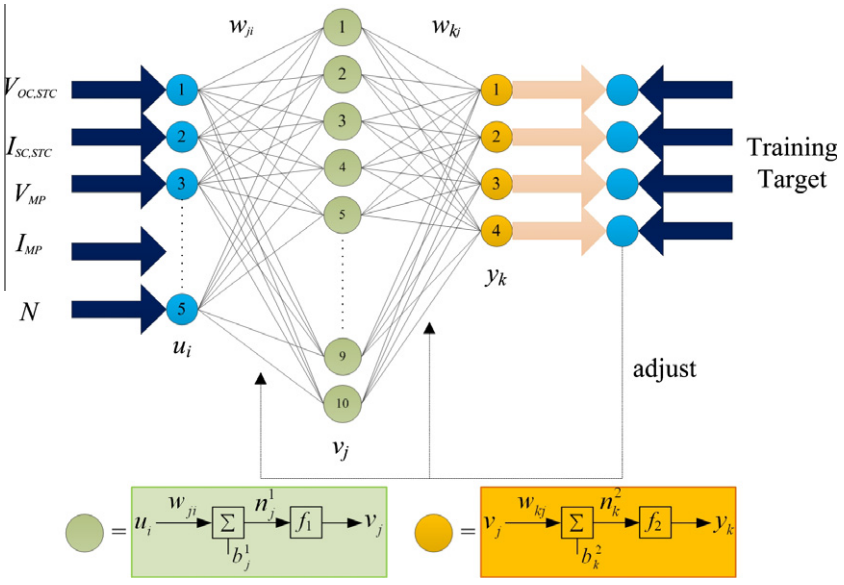

Fig. 5. Configuration of the utilized neural network.

$$n_k^2 = \sum_{j=1}^{10} w_{kj} v_j + b_k^2, \quad k = 1\text{–}4 \tag{8}$$

where w_{kj} is the weighting on the connection from the j th input unit, b_k^2 represent the bias for the second layer neurons. The output of the second layer is the network outputs of interest and these outputs are labeled as y_k

$$y_k = f_2(n_k^2), \quad f_2(x) = purelin(x) = x \tag{9}$$

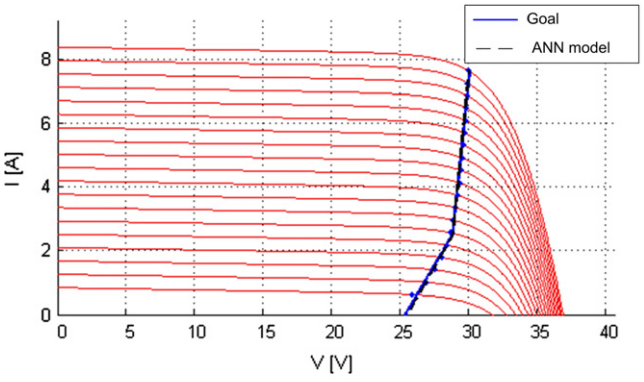

(a) PLS method.

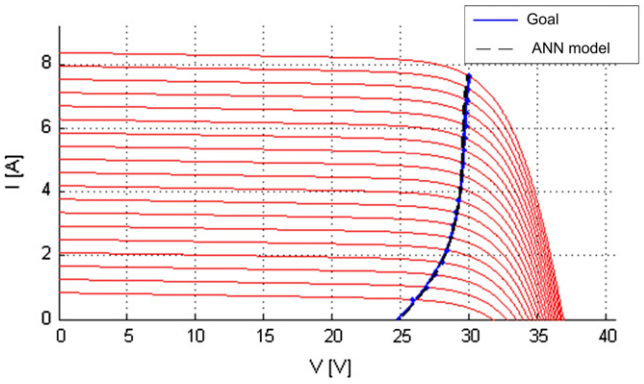

(b) CE method.

Fig. 6. Validation of the NN model.

In this study, all data are scaled to the range $\{-1; 1\}$, and pure linear transfer function is used as the activation function of both the hidden layer and output layers. Since the obtained NN will be implemented using a low-cost μC, using a linear function reduces the computational complexity. The proposed NN is trained using the commonly adopted back-propagation (BP) algorithm with the Levenberg–Marquardt optimization method. It is well-known that if a neural network is going to be effective, the training dataset must be complete enough. Therefore, all the solar panel data (total 294 data) collected from the top 10 solar panel producers of 2010 is utilized for training in this study. The collected data is first processed by the developed MATLAB program to obtain the corresponding EML parameter sets. Using the collected data as input of NN and the obtained EML parameter as output of NN, the proposed NN can be trained using the Neural Network Toolbox from MATLAB. The collected solar cell data and the trained results are also available at https://sites.google.com/site/d9707203/code.

In order to evaluate the performance of the developed NN model, the data of the utilized NU-U230F3 solar cell ($V_{OC,STC} = 37$, $I_{SC,STC} = 8.4$, $V_{MP} = 30$, $I_{MP} = 7.67$ and $N_S = 60$) is utilized as validation data. It should be noted that although the NU-U230F3 solar cell (from SHARP Corp.) utilized in this paper is also produced by the top 10 manufacturer, this data is excluded from the training

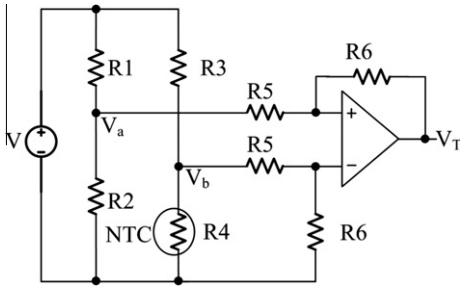

Fig. 8. Detailed implementation of the temperature compensation circuit.

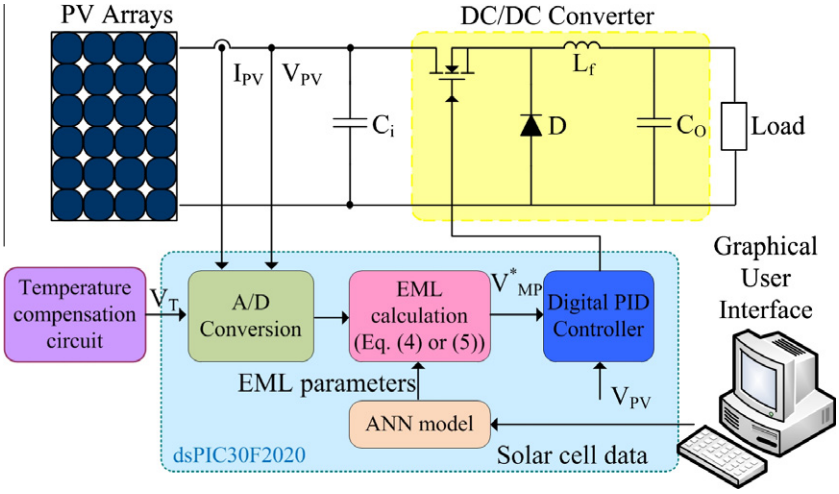

Fig. 7. Detailed implementation of the proposed method.

data. Fig. 6 illustrates the EML obtained from the accurate data and the NN model for PLS and CE cases. Observing Fig. 6, the EMLs obtained from the NN model are nearly identical to the ones obtained from the actual data in both cases. The mean square error (MSE) of the PLS and CE cases are 0.022 and 0.035, respectively. From Fig. 6, the proposed NN can be used to identify the parameters of EML for PLS and CE cases with a very high accuracy.

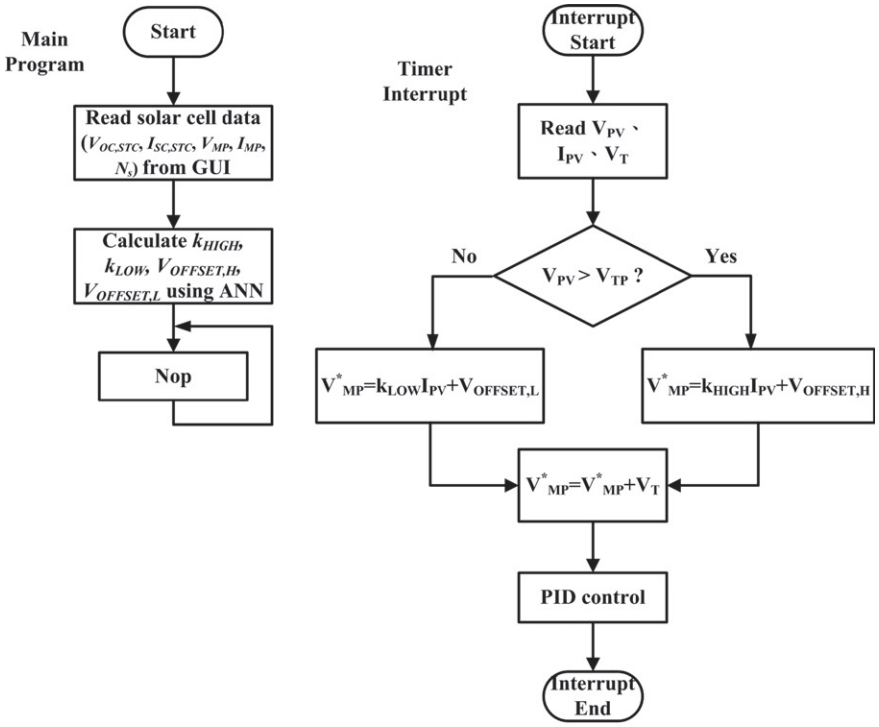

(a) PLS method.

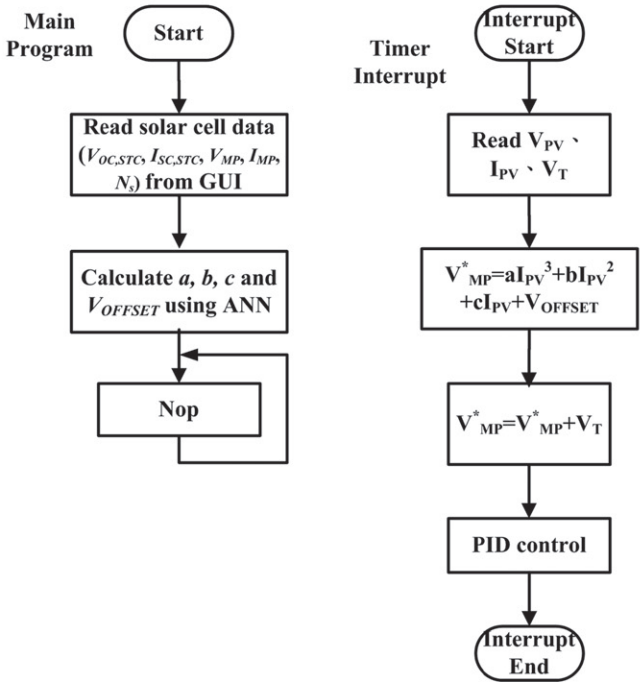

(b) CE method.

Fig. 9. Flowchart of the proposed MPPT methods.

5. Detailed description the proposed system

The block diagram illustrated in Fig. 4 has been implemented as shown in Fig. 7 where the complete converter and its control circuit are depicted in detail. From Fig. 7, the presented system consists of a PV panel, a DC/DC converter, a digital MPPT controller, a temperature compensation circuit and a GUI. In this paper, the PV panel employed is a mono-crystalline solar cell NU-U230F3. Most of the MPPT systems proposed in the literatures employ PWM-driven switch-mode power supply (SMPS) technologies. In this paper, a simple buck converter is used to interface the voltage from the PV panel to the load. The implementation of this part of circuit is conventional, therefore will not be discussed further here. From the literatures, the MPP locus will shift right/left if the operating temperature decreases/increases (Liu and Huang, 2011). Therefore, an additional temperature compensation voltage V_T which is proportional to the panel temperature should be added to the voltage command. This concept can be implemented using the circuit depicted in Fig. 8. In Fig. 8, the voltage V_T can be expressed as

$$V_T = (V_a - V_b) \times \frac{R6}{R5} \tag{10}$$

where $V_a = V_{REF} \cdot (R2/(R1 + R2))$ is a constant voltage. When panel temperature increases, the resistance $R4$ will decrease and V_b will reduce, resulting in a higher compensation voltage V_T. The resistor ratio $R6/R5$ controls the offset quantity of V_T, which can be determined by the temperature coefficient α_V provided by the manufacturer.

Fig. 9a shows the software flowchart of the proposed PLS method. From Fig. 9a, the proposed MPPT algorithm first reads the solar cell data from a simple GUI as shown in Fig. 10. Next, the NN developed in Section 4 will be embedded into the proposed digital MPPT controller and will be utilized to calculate parameters of the EML. After all the parameters are obtained, the main program goes into an infinite loop and waits for the timed interrupt. In the timer interrupt subroutine, the proposed MPPT method utilizes Eq. (4) to calculate a reference voltage command V_M^*P corresponding to an atmospheric condition using V_{PV} and I_{PV} as inputs. From Fig. 9a, the high irradiation EML should be employed when V_{PV} is greater than V_{TP}, otherwise the low irradiation EML should be used. Then, V_T is added to V_M^*P to compensate the temperature effect. After that, a high speed PID controller is used to regulate the PV panel voltage V_{PV} to follows V_M^*P, so that the DC/DC converter draws maximum power. Fig. 9b shows the software flowchart of the proposed CE method. From Fig. 9b, the operation principle of the CE method is similar to the PLS method, except for that the calculation of the V_M^*P is carried out using Eq. (5). In addition, there is no need to determine a turning point voltage V_{TP} because only

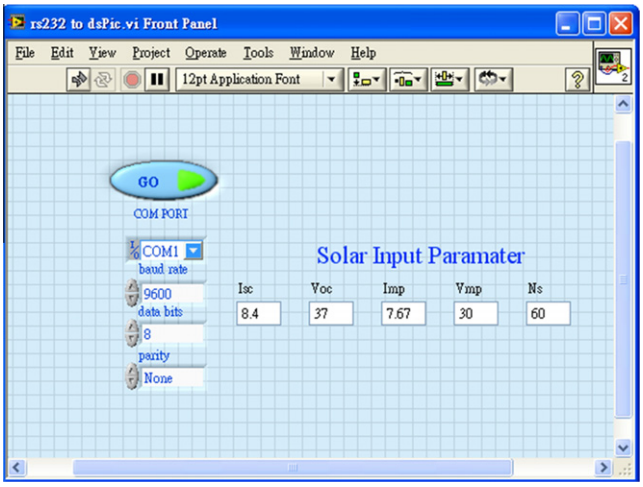

Fig. 10. A simple GUI.

Table 1
Parameters of the utilized PV panel.

NU-U230F3 (Configuration: 1 serial, 1 parallel)			
Maximum power (P_{max})	230 W	Short circuit current (I_{sc})	8.40 A
Open circuit voltage (V_{oc})	37.0 V	Maximum power current (I_{mp})	7.67 A
Maximum power voltage (V_{mp})	30.0 V	Temperature coefficient (α_v)	−0.129 V/°C

Table 2
Parameters of the implemented buck converter.

Component	C_i	C_o	L_f	Power switch	Diode
Type	330 μK	470 μF	330 μH	1RF540 N	STP10150

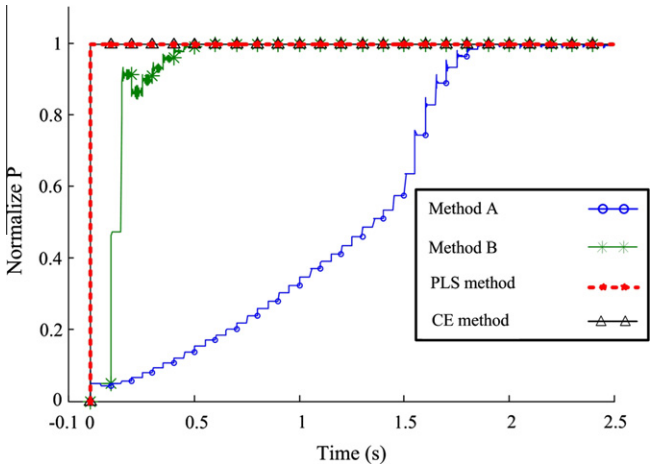

Fig. 11. Simulated starting waveform of four MPPT methods under standard test condition.

Table 3
Summary of the simulated results of four MPPT methods.

MPPT method	Method A	Method B	PLS	CE
$\eta_{DYNAMIC}$	98.48%	99.95%	99.96%	99.97%
Tracking time	0.367 s	0.293 s	0.007 s	0.007 s

one EML is utilized in CE method, this simplifies the design. It should be noted that the design procedures of both methods need not take the types of SMPS and voltage regulation loop into account. Therefore, the proposed MPPT method can be applied to all types of SMPS using different types of voltage regulating loops.

Table 4
Simulated tracking efficiencies of four MPPT methods under different irradiation conditions.

Irradiation (W/m^2)	Method A	Method B	PLS	CE
100	97.49	99.95	99.70	99.92
200	97.25	99.92	99.85	99.85
300	97. S9	99.97	99.72	99.95
400	97.86	99.90	99.94	99.92
500	97.42	99.96	99.99	99.99
600	97.15	99.99	99.92	99.97
700	97.75	99.98	99.99	99.95
800	97.54	99.98	99.98	99.98
900	98.26	99.94	99.94	99.99
1000	98.48	99.98	99.97	99.99

Table 5
The test pattern utilized in this paper. (Low irradiation level = 30%, High irradiation level = 100%).

Test no.	n	Slope (W/m^2)	Initial setting time (s)	t_1 (s)	t_2 (s)	t_3 (s)	t_4 (s)
Test 1	1	100	10	7	10	7	10
Test 2	1	50	10	14	10	14	10
Test 3	1	30	10	23	10	23	10
Test 4	1	20	10	35	10	35	10
Test 5	1	14	10	50	10	50	10
Test 6	1	10	10	70	10	70	10

6. Simulation and experimental results

To verify the correctness of the proposed MPPT methods, a 230 W prototyping circuit is implemented from which simulations and experiments are carried out accordingly. The configuration and parameters of the utilized PV panel and the implemented buck converter are listed in Tables 1 and 2, respectively. From Table 1, only one solar panel (NU-0230F3) is used in this study.

6.1. Simulation results

In this paper, the simulations are made using PSIM 9.0. Fig. 11 shows the start waveform of the conventional P&O method ($\Delta D = 1\%$ and $f_{MPPT} = 20$ Hz, denoted as method A), variable step-size P&O proposed in Pandey et al. (2008) (denoted as method B), the proposed PLS method and the proposed CE method for standard test conditions of 1000 W/m^2 solar irradiance and 25 °C PV panel temperature. Table 3 summarizes the simulated rise time and static MPP tracking efficiency of these four MPPT methods. From Fig. 11 and Table 3, the proposed PLS and CE method can reach the MPP much faster than method A and method B. It can also be observed that the oscillation around the MPP is very small thus can be neglected. The simulated static tracking efficiencies of these four methods under different irradiation conditions are summarized in Table 4.

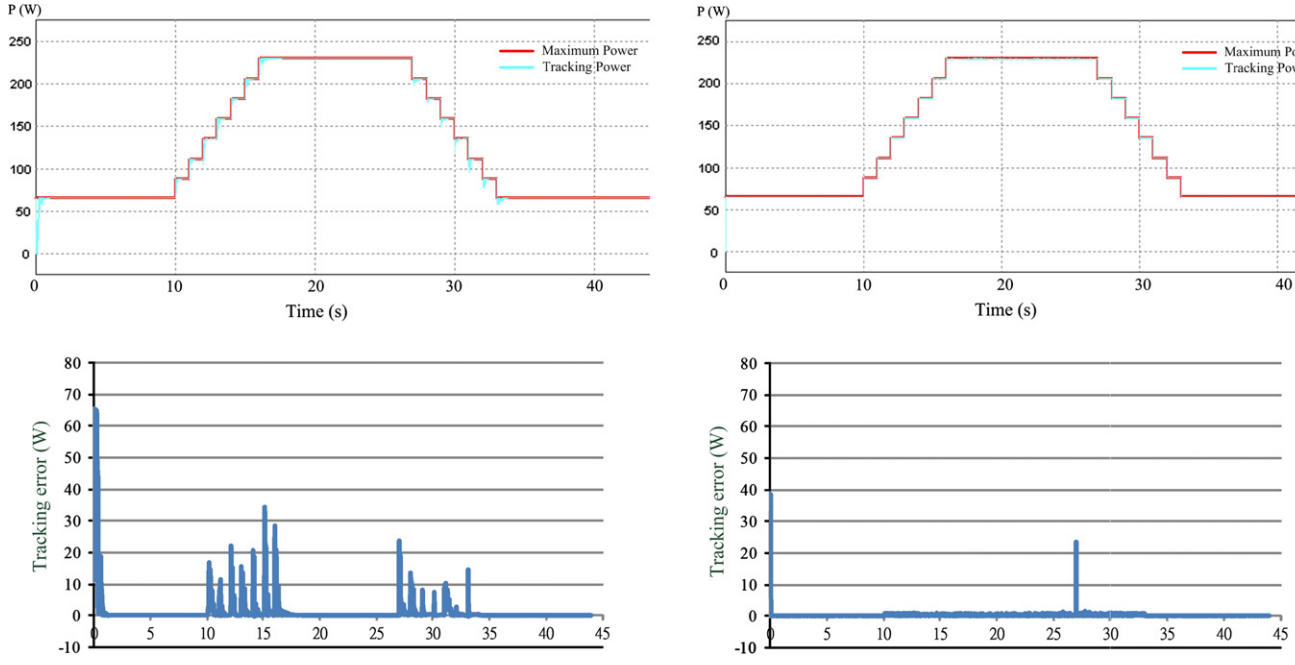

(a) Method B. (b) PLS method.

Fig. 12. Simulated dynamic tracking waveforms.

The simulations of the dynamic MPP tracking efficiency of these four methods are also carried out. The complete EN50530 tests contain two test sequences of different irradiance level. The first sequence covers the interval from 10% to 50%, while the second sequence covers the irradiance from 30% to 100% of standard test conditions (EN 50530, 2010). In this paper, only the test patterns in the second test sequence are performed. The test patterns utilized in this paper are summarized in Table 5. In this paper, only part of the simulated waveforms is presented. Fig. 12 shows the simulated tracking waveform of method B and the proposed PLS method for the test pattern #1 (the test pattern with the highest irradiance variation slope). The simulation result of the CE method is similar to that of the PLS method, therefore is omitted here. The simulated dynamic MPP tracking efficiencies are outlined in Table 6. From Table 6, the simulated $\eta_{DYNAMIC}$ for method A and method B is lower than the proposed methods for all the test patterns owing to the oscillations around MPP (method A) and the slow MPP tracking of the algorithm (method A and B). Also from Table 6, the performance improvement of the proposed method for higher slope tests is more significant than that for lower slope tests.

Table 6
Simulated dynamic MPP tracking efficiencies of four MPPT methods.

$\eta_{DYNAMIC}$	Method A (%)	Method B (%)	PLS (%)	CE (%)
Test 1	95.00	97.48	99.67	99.85
Test 2	96.32	98.28	99.85	99.93
Test 3	97.20	98.74	99.90	99.96
Test 4	97.65	99.00	99.93	99.97
Test 5	97.83	99.15	99.95	99.98
Test 6	98.02	99.25	99.97	99.99

Table 7
Tracking efficiencies of four MPPT methods under different irradiation conditions.

Irradiation (W/m^2)	Method A	Method B	PLS	CE
100	96.01	99.89	99.69	99.90
200	95.21	99.88	99.85	99.85
300	96.02	99.96	99.69	99.95
400	96.55	99.89	99.92	99.88
500	94.48	99.95	99.99	99.99
600	95.21	99.99	99.89	99.98
700	94.88	99.98	99.99	99.93
800	95.75	99.99	99.99	99.98
900	95.37	99.95	99.92	99.99
1000	95.39	99.99	99.95	99.99

6.2. Experimental results

A prototyping circuit using the parameters shown in Tables 1 and 2 is also constructed. The proposed algorithms are validated using the Chroma Solar Array Simulator 6205 in SAS mode. For comparison, method A and method B are also implemented using the same hardware specification. Using the prototyping circuits, static MPPT efficiency tests are carried out. Table 7 summarizes the measured static tracking efficiencies of these four methods under different irradiation conditions. The experiments of the dynamic MPP tracking efficiency of these four methods are also carried out using the prototyping circuits. The test patterns utilized for these experiments are the same as the one used for simulation. Fig. 13 shows the measured

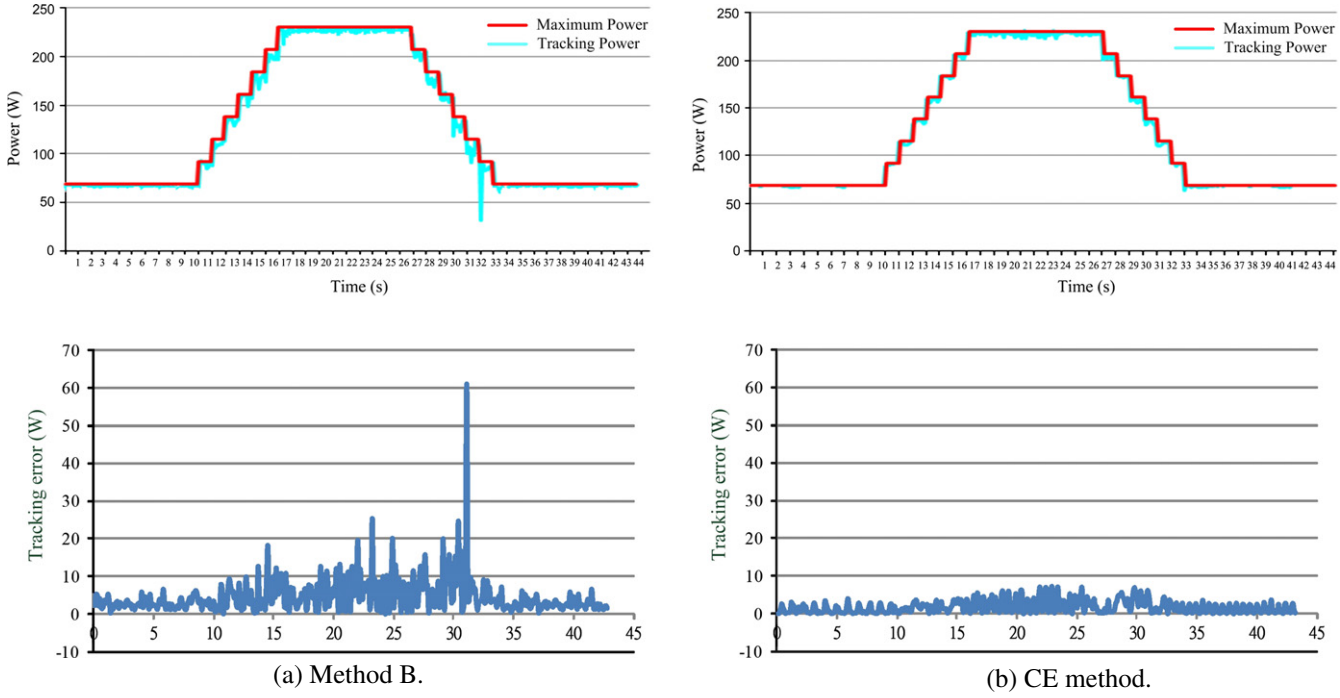

Fig. 13. Measured s dynamic tracking waveforms.

Table 8
Measured dynamic MPP tracking efficiencies of four MPPT methods.

$\eta_{DYNAMIC}$	Method A (%)	Method B (%)	PLS (%)	CE (%)
Test 1	93.85	96.44	98.63	98.79
Test 2	94.17	97.78	99.32	99.40
Test 3	94.30	98.48	99.59	99.64
Test 4	94.90	98.79	99.73	99.76
Test 5	95.26	99.00	99.81	99.83
Test 6	95.50	99.13	99.86	99.88

dynamic tracking waveforms for method B and the proposed CE method for the test pattern #1, respectively. The dynamic tracking waveform of the PLS method is nearly identical to that of the CE method, therefore is omitted here. For method A and B, the time step for one perturbation is set as 50 ms ($f_{MPPT} = 20$ Hz). From Fig. 13, it can be observed that apart from better overall MPP tracking with smaller oscillations in steady state, tracking with the proposed algorithm clearly displays faster dynamics. The measured dynamic MPP tracking efficiencies are outlined in Table 8.

6.3. Discussions

According to the simulation and experimental results, the proposed methods exhibit higher dynamic MPP tracking efficiency and faster tracking speed than method A and method B. Although the performance improvement of the proposed method for higher slope tests is more significant than that for lower slope tests, the dynamic tracking efficiencies of the proposed methods are all higher than method A and method B for all test cases.

The comparison between the proposed PLS method and the CE method can be briefly discussed as follows. The computation burden of the PLS method (one multiplication and one addition) is slightly lower than the CE method (six multiplications and three additions). In addition, the PLS method can be realized using only analog components such as operational amplifiers. However, the turning point voltage V_{TP} should be determined first for PLS method. (In this paper, the turning point irradiation is set as 300 W/m^2.) Since the optimal setting of this value varies when the panel is different, using a constant value will somewhat reduce the tracking efficiency. Therefore, the performance of CE method will be slightly better than that of the PLS method (see Tables 4 and 7).

7. Conclusion

In this paper, two digital MPPT methods for fast changing environments are proposed. A neural network (NN)-based program which can be used to calculate the parameters of the emulated MPP locus is also developed and embedded into the proposed digital MPPT system to make the developed system more convenient for common PGS users. By using piecewise line segments or cubic equation to approximate the MPP locus, high static and dynamic tracking efficiencies as well as fast tracking speed can be achieved. Simulation and experimental results are also provided to demonstrate the effectiveness of the proposed techniques. The main advantages of the proposed MPPT methods are the following:

(1) The tracking speed is fast due to the utilization of high speed voltage regulation loop, resulting high dynamic MPP tracking efficiency.
(2) The proposed methods are very simple because they require only a few multiplication and addition operations; hence, implementation using low-cost μC is achievable.
(3) The static MPP tracking efficiencies of the proposed methods are very high because, at steady-state, there are no oscillations around the MPP.
(4) The proposed methods can be applied to all types of power converters, and can easily be integrated into any type of voltage regulation loop.
(5) Using the developed NN model, the PGS user can apply the developed MPPT controller to any PV panel without the need to modify the firmware of the PGS.

References

Abdelsalam, A.K., Massoud, A.M., Ahmed, S., Enjeti, P.N., 2011. High-performance adaptive perturb and observe MPPT technique for photovoltaic-based microgrids. IEEE Trans. Power Electron. 26, 1010–1021.

Alajmi, B.N., Ahmed, K.H., Finney, S.J., Williams, B.W., 2011. Fuzzy-logic-control approach of a modified hill-climbing method for maximum power point in microgrid standalone photovoltaic system. IEEE Trans. Power Electron. 26, 1022–1030.

Andrejašič, T., Jankovec, M., Topič, M., 2011. Comparison of direct maximum power point tracking algorithms using EN 50530 dynamic test procedure. IET Renew. Power Gener. 5, 281–286.

Brunton, S.L., Rowley, C.W., Kulkarni, S.R., Clarkson, C., 2010. Maximum power point tracking for photovoltaic optimization using ripple-based extremum seeking control. IEEE Trans. Power Electron. 25, 2531–2540.

Chekired, F., Larbes, C., Rekioua, D., Haddad, F., 2011. Implementation of a MPPT fuzzy controller for photovoltaic systems on FPGA circuit. Energy Procedia 6, 541–549.

Chen, C., Duan, S., Cai, T., Liu, B., 2011. Online 24-h solar power forecasting based on weather type classification using artificial neural network. Solar Energy 85, 2856–2870.

Du, Y., Lu, D.D.-C., 2011. Battery-integrated boost converter utilizing distributed MPPT configuration for photovoltaic systems. Solar Energy 85, 1992–2002.

Elgendy, M.A., Zahawi, B., Atkinson, D.J., 2012. Assessment of perturb and observe MPPT algorithm implementation techniques for PV pumping applications. IEEE Trans. Sust. Energy 3, 21–33.

EN 50530, 2010. Overall efficiency of grid connected photovoltaic inverters.

Esram, T., Chapman, P.L., 2007. Comparison of photovoltaic array maximum power point tracking techniques. IEEE Trans. Energy Convers. 22, 439–449.

Hohm, D.P., Ropp, M.E., 2003. Comparative study of maximum power point tracking algorithms. Prog. Photovoltaic's: Res. Appl. 11, 47–62.

Jain, S., Agarwal, V., 2004. A new algorithm for rapid tracking of approximate maximum power point in photovoltaic systems. IEEE Trans. Power Electron. 2, 16–19.

Kakosimos, P.E., Kladas, A.G., 2011. Implementation of photovoltaic array MPPT through fixed step predictive control technique. Renew. Energy 36, 2508–2514.

Kassem, A.M., 2012. MPPT control design and performance improvements of a PV generator powered DC motor-pump system based on artificial neural networks. Electr. Power Energy Syst. 43, 90–98.

Kimball, J.W., Krein, P.T., 2008. Discrete-time ripple correlation control for maximum power point tracking. IEEE Trans. Power Electron. 23, 2353–2362.

Ko, S.H., Chao, R.M., 2012. Photovoltaic dynamic MPPT on a moving vehicle. Solar Energy 86, 1750–1760.

Lalili, D., Mellit, A., Lourci, N., Medjahed, B., Berkouk, E.M., 2011. Input output feedback linearization control and variable step size MPPT algorithm of a grid-connected photovoltaic inverter. Renew. Energy 36, 3282–3291.

Lee, C.Y., Chen, P.H., Shen, Y.X., 2011. Maximum power point tracking (MPPT) system of small wind power generator using RBFNN approach. Expert Syst. Appl. 38, 12058–12065.

Leconte, A., Achard, G., Papillon, P., 2012. Global approach test improvement using a neural network model identification to characterise solar combisystem performances. Solar Energy 86, 2001–2016.

Liu, F., Duan, S., Liu, F., Liu, B., Kang, Y., 2008. A variable step size INC MPPT method for PV systems. IEEE Trans. Ind. Electron. 55, 2622–2628.

Liu, Y.H., Huang, J.W., 2011. A fast and low cost analog maximum power point tracking method for low power photovoltaic systems. Elsevier Solar Energy 85, 2771–2780.

Masoum, M.A., Dehbonei, H., Fuchs, E.F., 2002. Theoretical and experimental analyses of photovoltaic systems with voltage- and current-based maximum power-point tracking. IEEE Trans. Energy Convers. 17, 514–522.

Mei, Q., Shan, M., Liu, L., Guerrero, J.M., 2011. A novel improved variable step-size incremental-resistance MPPT method for PV systems. IEEE Trans. Ind. Electron. 58, 2427–2434.

Mutoh, N., Ohno, M., Inoue, T., 2006. A method for MPPT control while searching for parameters corresponding to weather conditions for PV generation systems. IEEE Trans. Ind. Electron. 53, 1055–1065.

Pai, F.S., Chao, R.M., Ko, S.H., Lee, T.S., 2011. Performance evaluation of parabolic prediction to maximum power point tracking for PV array. IEEE Trans. Sust. Energy 2, 60–68.

Pandey, A., Dasgupta, N., Mukerjee, A.K., 2008. High-performance algorithms for drift avoidance and fast tracking in solar MPPT system. IEEE Trans. Energy Convers. 23, 681–689.

Salas, V., Olías, E., Barrado, A., Lázaro, A., 2006. Review of the maximum power point tracking algorithms for stand-alone photovoltaic systems. Solar Energy Mater. Solar Cells 90, 1555–1578.

Sera, D., Teodorescu, R., Hantschel, J., Knoll, M., 2008. Optimized Maximum Power Point Tracker for Fast-Changing Environmental Conditions. IEEE Trans. Ind. Electron. 55, 2629–2637.

Sokolov, M., Shmilovitz, D., 2008. A modified MPPT scheme for accelerated convergence. IEEE Trans. Energy Convers. 23, 1105–1107.

Syafaruddin, Karatepe, E., Hiyama, T., 2012. Performance enhancement of photovoltaic array through string and central based MPPT system under non-uniform irradiance conditions. Energy Convers. Manage. 62, 131–140.

Villalva, M.G., Gazoli, J.R., Filho, E.R., 2009. Comprehensive approach to modeling and simulation of photovoltaic arrays. IEEE Trans. Power Electron. 24, 1198–1208.

Xiao, W., Dunford, W.G., Palmer, P.R., Capel, A., 2007. Application of centered differentiation and steepest descent to maximum power point tracking. IEEE Trans. Ind. Electron. 54, 2539–2549.